Quantum Induced Coherence Light Detection and Ranging

Gewei Qian,[1] Xingqi Xu,[1,*] Shun-An Zhu,[1] Chenran Xu,[1] Fei Gao,[2] V. V. Yakovlev,[3] Xu Liu,[1] Shi-Yao Zhu,[1,4] and Da-Wei Wang[1,4,5,†]

[1]*Interdisciplinary Center for Quantum Information, State Key Laboratory of Modern Optical Instrumentation, and Zhejiang Province Key Laboratory of Quantum Technology and Device, School of Physics, Zhejiang University, Hangzhou 310027, Zhejiang Province, China*

[2]*ZJU-Hangzhou Global Science and Technology Innovation Center, College of Information Science and Electronic Engineering, Zhejiang University, Hangzhou 310027, China*

[3]*Texas A&M University, 3120 TAMU, College Station, Texas 77843, USA*

[4]*Hefei National Laboratory, Hefei 230088, China*

[5]*CAS Center for Excellence in Topological Quantum Computation, University of Chinese Academy of Sciences, Beijing 100190, China*

(Received 5 February 2023; accepted 22 June 2023; published 18 July 2023)

Quantum illumination has been proposed and demonstrated to improve the signal-to-noise ratio (SNR) in light detection and ranging (LiDAR). When relying on coincidence detection alone, such a quantum LiDAR is limited by the timing jitter of the detector and suffers from jamming noise. Inspired by the Zou-Wang-Mandel experiment, we design, construct, and validate a quantum induced coherence (QuIC) LiDAR which is inherently immune to ambient and jamming noises. In traditional LiDAR the direct detection of the reflected probe photons suffers from deteriorating SNR for increasing background noise. In QuIC LiDAR we circumvent this obstacle by only detecting the entangled reference photons, whose single-photon interference fringes are used to obtain the distance of the object, while the reflected probe photons are used to erase path information of the reference photons. In consequence, the noise accompanying the reflected probe light has no effect on the detected signal. We demonstrate such noise resilience with both LED and laser light to mimic the background and jamming noise. The proposed method paves a new way of battling noise in precise quantum electromagnetic sensing and ranging.

DOI: 10.1103/PhysRevLett.131.033603

Quantum properties of light can be used to improve the signal-to-noise ratio (SNR) in light detection and ranging (LiDAR) by implementing quantum illumination (QI) and correlation detection [1–13]. One of the entangled photons serves as a reference while the other photon is sent to probe the object. The spatial and temporal correlation of entangled photons are used to extract the image and distance of the object based on joint measurement [14–17]. The extra information provided by the reference photons significantly improves the SNR in noisy and lossy environment [18–21] [see Figs. 1(a) and 1(b)]. However, in such QI LiDAR the noise from the object still enters the detector, which can be jammed by saturation illumination.

In this Letter, we use quantum induced coherence (QuIC), which was first demonstrated in the Zou-Wang-Mandel (ZWM) experiment [28] and recently used to image objects with undetected photons [29–34], to solve the noise problems in LiDAR. In the ZWM experiment, entangled photons are generated in the spontaneous parametric down conversion (SPDC) of two nonlinear crystals. The single-photon interference of the signal photons depends on whether we in principle know which crystal generates the photon pairs. According to the principle of quantum eraser, if the idler photons leak which-way information of the signal photons, the interference disappears, while erasing such information brings on the interference [35–37]. This mechanism has been used in spectroscopy [38–40], optical coherence tomography (OCT) [41–44], and holography [45], where infrared imaging and spectroscopy are achieved with visible light detectors. Here, we show that QuIC can fundamentally improve the noise resilience of LiDAR. Without coincidence detection, we obtain the distance and image of the object by only detecting the locally kept reference photons, while the entangled probe photons reflected from the object are used to erase which-way information of the reference photons. In such a scheme the background noise and jamming light have no direct effect on our detection [Fig. 1(c)]. We demonstrate the ranging and imaging ability of QuIC LiDAR and show its robustness in LED and laser noise.

Three light beams are used to build the QuIC LiDAR. A pump laser beam pumps a periodically poled lithium niobate (PPLN) crystal, which generates a probe beam and a reference beam in SPDC. Both the pump and reference beams are kept as local while the probe beam is sent out to

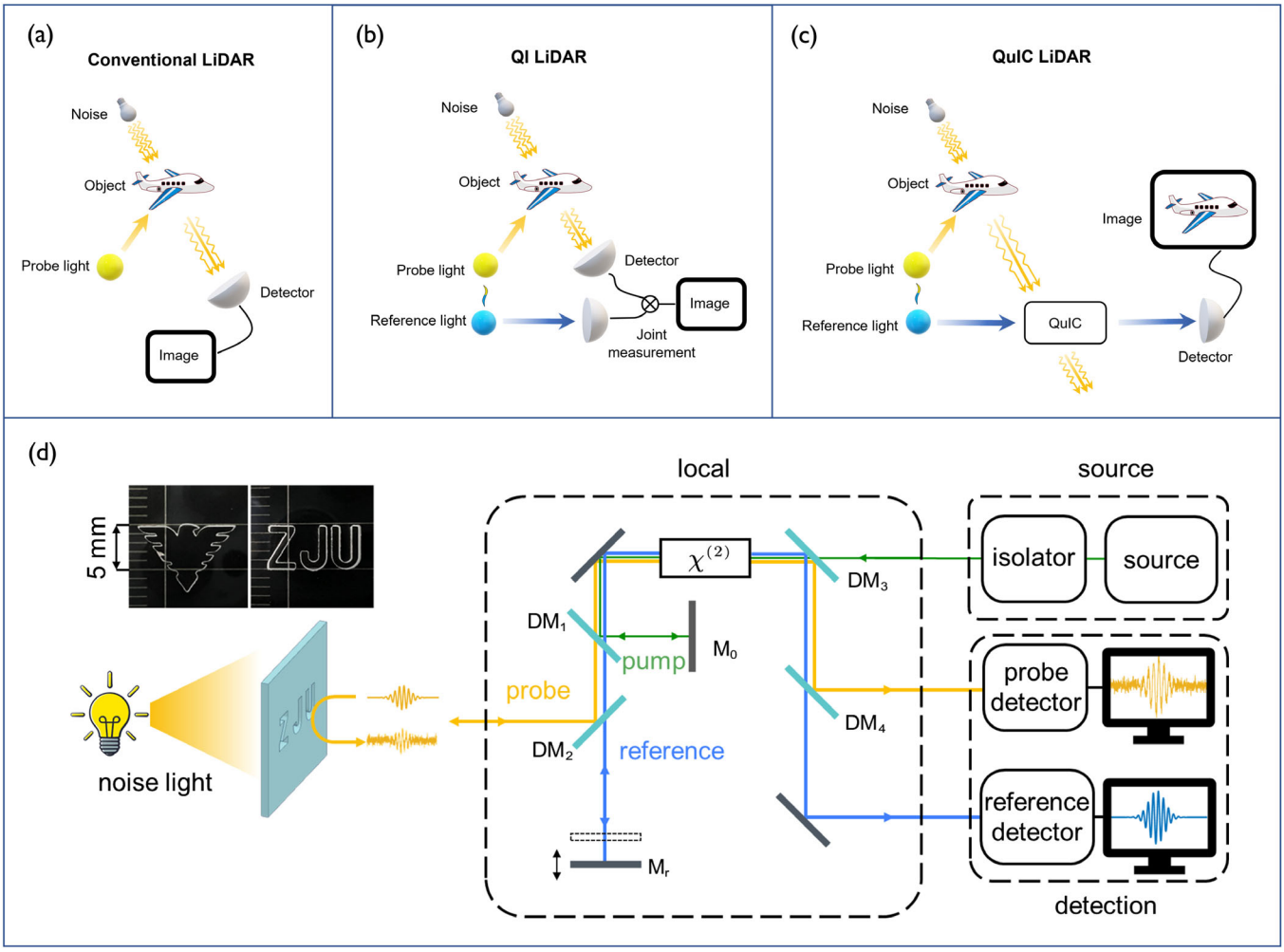

FIG. 1. Physical principles for conventional, QI and QuIC LiDARs. (a) Conventional LiDAR. (b) QI LiDAR, where the SNR is enhanced by joint measurement. (c) QuIC LiDAR. Without detecting the probe light, a locally kept reference light is detected to obtain the distance of the object, enabled by QuIC. (d) The setup consists of three modules (enclosed in dashed lines), the pump laser, the local scanning module and the detection module. A collimated 532 nm laser (green line, 10 kHz linewidth) is used to pump a type-0 PPLN crystal (2 cm length) to generate SPDC entangled reference (blue line) and probe (yellow line) photons centered at 893 and 1316 nm wavelength. The two light beams are separated by a dichroic mirror DM_2. The reference beam is reflected by a scanning mirror M_r. All reflected beams go through the crystal a second time. We detect the reference beam with a Si-based CMOS camera. The probe light is also detected with an InGaAs camera to compare the performance of QuIC and conventional LiDAR. An off-axis parabolic mirror and plano-convex lenses are used for the imaging setup (see [22] for details).

detect the object. The probe beam reflected from the object is collected to go through the nonlinear crystal a second time together with the locally reflected pump and reference beams in a Michelson configuration [46] of the ZWM experiment [28] [see Fig. 1(d)]. The light intensity of the reference beam at the detector (see Supplemental Material [22]),

$$I_r \propto \eta^2[1+\gamma(\tau)|r_p|\cos(\phi_p+\phi_r-\phi_0)], \tag{1}$$

where η is the probability amplitude of generating an entangled photon pair in a single pass through the nonlinear crystal, r_p is the reflection coefficient of the object, ϕ_p, ϕ_r, and ϕ_0 are the accumulated phases of the probe, reference, and pump beams in the round loops from leaving to returning to the PPLN crystal. Here, we assume $\gamma(\tau)=\exp(-\tau^2/2\sigma^2)$ to be the overlapping function between the returned probe and reference light modes with τ being their traveling time difference and σ the coherence time of the SPDC light. We obtain the distance of the object by scanning the light path of the reference beam to achieve maxima in the interference visibility,

$$V=|r_p|\gamma(\tau). \tag{2}$$

This strategy of extracting distance from the visibility rather than the phases can be regarded as a quantum version of the white light interferometry [47]. The

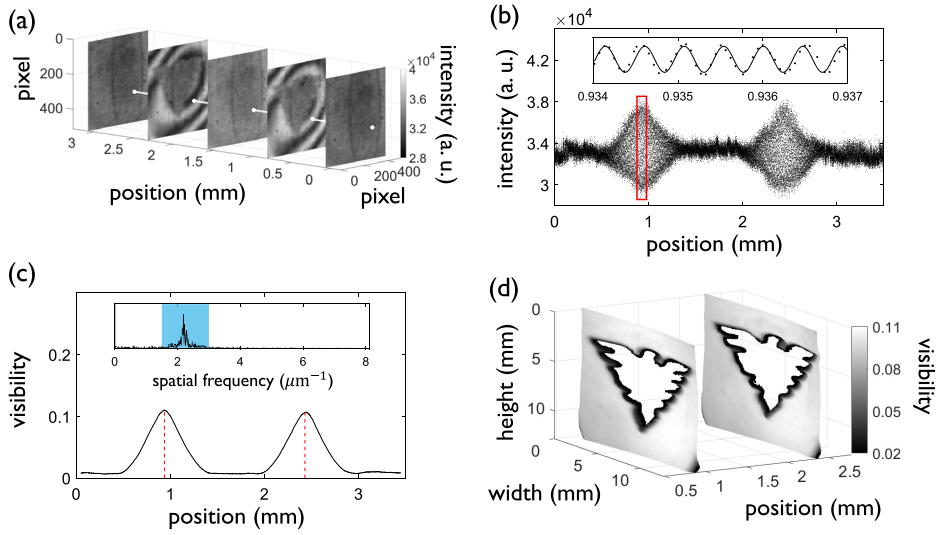

FIG. 2. Ranging of QuIC LiDAR. (a) Real-time images captured by the CMOS camera during the scanning of M_r. The two images carrying interference patterns correspond to the two faces of the plate. The exposure time of each image is 50 ms. The scanning step is 60 nm with a total scanning length 3.5 mm. (b) Interference fringes along the white lines in (a). The inset shows the interference fringes in a region within the red rectangle. (c) Interference visibility obtained from STFT with an integration window 100 μm. The step in the horizontal axis is 1 μm. Inset: the Fourier transform of the interference in the red frame in (b). The Fourier transform intensity in the spatial frequency range from 1.5 to 3 μm^{-1} (blue shaded area) is used to extract the visibility (see [22] for detail). The two peaks in the main frame with the weights being marked by red dashed lines indicate the positions of the two surfaces. (d) Images and positions of the two silica plate faces obtained from QuIC LiDAR. We plot the visibility as functions of the positions of the STFT weights recorded on the reference camera during the delay scan. The thickness of the silica plate is 1.01 ± 0.01 mm. The optical path between the two faces measured from QuIC LiDAR is 1.499 ± 0.009 mm.

visibility in QuIC LiDAR is proportional to $|r_p|$, i.e., linear with the amplitude reflectivity of the object [48], which makes QuIC LiDAR advantageous in detecting surfaces with low reflectivity.

The performance of QuIC LiDAR is tested with two silica plates with hollowed symbols [Fig. 1(d)]. We scan the reference light path to observe its interference patterns on a CMOS camera. We find two such positions which correspond to the two surfaces of the silica plates [see Figs. 2(a) and 2(b)]. The envelopes of the interference fringes during the scanning have a maximum visibility 0.11 and a spatial width 0.4 mm, which sets a limit on the ranging resolution [49]. While no interference filter is used in the experiment, the interference envelope is larger than the coherence length of the SPDC light (16.5 μm) because each pixel of the camera only covers part of the SPDC spectra. In order to filter the scanning noise in determining the distance of the object, we perform short-time Fourier transform (STFT) with a scanning window 100 μm to obtain the visibility [Fig. 2(c)]. The weights of the two peaks are regarded as the expected distances of the two surfaces. In Fig. 2(d), the distances and images of the two plate faces are obtained with a lateral resolution 430 μm and a ranging accuracy 3.9 μm (see [22]) by locating the STFT weights on each pixel [41,42,50].

While QI can significantly enhance the SNR [3,18], its performance in LiDAR quickly deteriorates when the background noise increases to the same level of the signal. It is also prone to jamming since all photons from the object are detected [see Fig. 1(b)]. In QuIC LiDAR, the position of the object is obtained by detecting the local reference light instead of the reflected probe light [see Fig. 1(c)], such that the ambient noise accompanying the probe light has no effect in our detection. We test such noise resilience by shining the sample from behind with an LED light and a laser, which both have wavelengths similar to that of the probe light. In order to make a comparison, we also extract the images from the probe light following the same procedure as that of the reference light to mimic the performance of ordinary OCT. Without background noise, the two images extracted from the reference and probe light cameras are similar except for a slight difference in resolution [51] [Figs. 3(a) and 3(b)]. To simulate strong background noise, we focus the LED light to a small area of the object. The spectrum power density of the LED is about 7 $mW/m^2/nm$, much lower than that of the Sun (300 $mW/m^2/nm$). As a result, the noise enters the probe light camera and substantially obscures the image area illuminated by the LED light [Fig. 3(d)], while no difference is detected by the reference light camera [Fig. 3(c)].

The only practical way to jam QuIC LiDAR is to send a laser back to the local module to induce the stimulated parametric down conversion (PDC) in the crystal [see the black spot in Fig. 3(e)]. However, such jamming requires

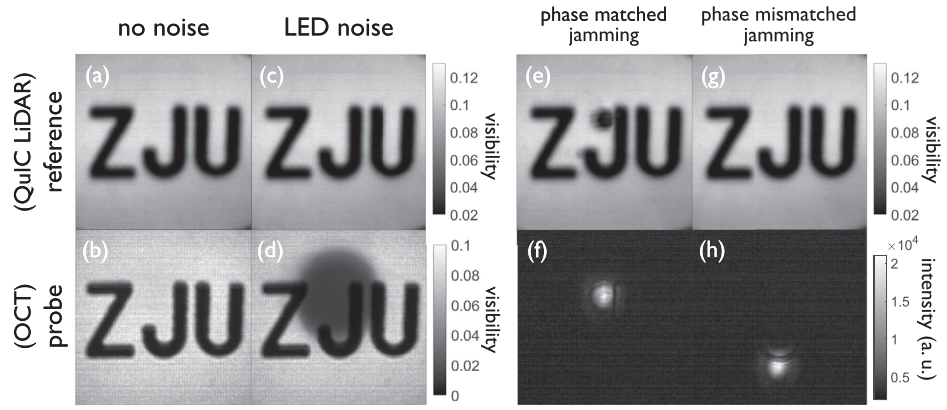

FIG. 3. Noise robustness of QuIC LiDAR. The images in the upper (lower) row are extracted from the reference (probe) light cameras. (a) and (b) are images without added noise. (c) and (d) are images in LED noise. (e)–(h) are images in jamming laser noise. (e) and (f) satisfy the phase matching condition while (g) and (h) do not. The powers of the reflected probe beam, the LED light and the laser before entering the probe camera are 72 nW, 44 nW, and 2.6 μW. The exposure time is 6 ms for (a), (c), (e) and (g), 15 ms for (b) and (d), and 20 μs for (f) and (h). Here, (f) and (h) are unprocessed images from the probe camera. The reference image has lower resolution than the probe image due to the imperfection of the transverse phase matching in the crystal, which is restricted by the crystal aperture and the pump beam waist size [51].

that the pump and jamming lasers have to overlap in space, be colinear and phase matching. As a result, the jamming is only efficient in specific directions covering a few pixels, leaving other pixels undisturbed. Such a strict requirement on phase-matching allows us to avoid laser jamming by adjusting the orientation or the temperature of the crystal [Fig. 3(g)]. In comparison, the probe light camera can be easily jammed by the laser [see Figs. 3(f) and 3(h)].

To quantitatively characterize the noise robustness of QuIC LiDAR, we measure the SNR, $\mathcal{F}_s/\mathcal{F}_n$, where $\mathcal{F}_s$ and $\mathcal{F}_n$ are the value of signal peak and noise baseline in the Fourier transform spectrum (see Fig. S4 in Supplemental Material [22]), at different noise levels defined in decibel, $10\log_{10}(P_n/P_p)$, where P_n and P_p are the intensities of the noise and reflected probe light, respectively (see Fig. 4). We compare the SNR of the interference of the probe and reference light to quantify the advantage of QuIC LiDAR in noise resilience. For the LED noise, the SNR of the probe light starts dropping at a noise level 23.4 dB until going below the detection line at 36 dB, while the SNR of the reference light is unaffected [see Fig. 4(a)]. For laser jamming, the stimulated PDC light at the phase matching direction can reduce the SNR of the reference light to 1 with a laser noise 43.7 dB. However, for mismatching pixels the SNR remains unaffected [Fig. 4(b)].

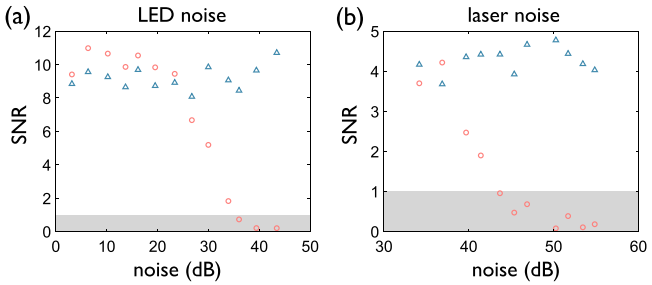

FIG. 4. The SNR of QuIC LiDAR in LED (a) and laser (b) noises. In (a), we compare the SNR in QuIC LiDAR (blue triangles) and in direct detection of the probe light (red circles). For noise level below 23.4 dB, the LED noise is weaker than the systematic noise, such that the SNR of the probe light remains unchanged. For higher LED noise, the SNR of the probe light decreases, while the one of the QuIC LiDAR remains unchanged. In (b), we simulate saturation jamming by sending a laser back to the crystal, which induces stimulated PDC noise. The red circles and blue triangles are the SNRs of the reference light in the areas satisfying and violating the phase matching condition. The intensities of probe and noise light are measured by an InGaAs power meter with an iris covering the region of interest on the camera.

In conclusion, we demonstrate that QuIC LiDAR has superior noise resilience compared with the QI LiDAR that relies on coincidence detection. With the freedom in selecting wavelengths in SPDC [33], we can build midinfrared and terahertz QuIC LiDAR by using proper crystals (e.g., $AgGaS_2$ for midinfrared up to 13 μm) [38,52–54]. In such wavelengths the LiDAR detection is better concealed and difficult to jam because efficient detectors and lasers are rare. For applications in microwave regime where background noise brings a huge challenge, we can integrate the microwave-to-optics conversion [17,55,56] to the current design or use microwave-optical entangled light sources [57]. The QuIC LiDAR described here can be integrated with on-chip entangled photon sources and delay lines [58] to make it small and compact to be used in modern transportation vehicles. A common problem for QI based LiDAR is the necessity of delaying or storing the reference photons [6,59], which may bring difficulty in scenarios of conventional

LiDAR. To meet this challenge, we need to use fast delay-scanning techniques [60–62]. The weak intensity of SPDC light makes it difficult to detect objects with low reflection. A solution to this problem is to push the idea to the classical regime, i.e., by adding a seed to our current setup to build an SU(1,1) interferometer [63,64] to improve the SNR in cost of the ranging accuracy.

We thank Ruosong Mao and Weiru Fan for helpful discussion. This work was supported by the National Natural Science Foundation of China (Grant No. 11934011), Zhejiang Province Key Research and Development Program (Grant No. 2020C01019), the Strategic Priority Research Program of Chinese Academy of Sciences (Grant No. XDB28000000), and the Fundamental Research Funds for the Central Universities. F. G. acknowledges the support from National Key Research and Development Program of China (Grant No. 2022YFA1404902) and National Natural Science Foundation of China (Grant No. 62171406). V. V. Y. acknowledges partial support from the NSF (No. CMMI-1826078), AFOSR (No. FA9550-20-1-0366), and NIH (No. 1R01GM127696, No. 1R21GM142107, No. 1R21CA269099).

*xuxingqi@zju.edu.cn
†dwwang@zju.edu.cn

[1] V. Giovannetti, S. Lloyd, and L. Maccone, Nature (London) **412**, 417 (2001).
[2] V. Giovannetti, S. Lloyd, and L. Maccone, Phys. Rev. A **65**, 022309 (2002).
[3] S. Lloyd, Science **321**, 1463 (2008).
[4] L. Maccone and C. Ren, Phys. Rev. Lett. **124**, 200503 (2020).
[5] S.-H. Tan, B. I. Erkmen, V. Giovannetti, S. Guha, S. Lloyd, L. Maccone, S. Pirandola, and J. H. Shapiro, Phys. Rev. Lett. **101**, 253601 (2008).
[6] J. H. Shapiro, IEEE Aerospace Electron. Syst. Mag. **35**, 8 (2020).
[7] R. Nair and M. Gu, Optica **7**, 771 (2020).
[8] M. Lanzagorta, Synth. Lect. Quantum Comput. **3**, 1 (2011).
[9] M. M. Wilde, M. Tomamichel, S. Lloyd, and M. Berta, Phys. Rev. Lett. **119**, 120501 (2017).
[10] M. Sanz, U. Las Heras, J. J. García-Ripoll, E. Solano, and R. Di Candia, Phys. Rev. Lett. **118**, 070803 (2017).
[11] Z. Zhang, M. Tengner, T. Zhong, F. N. C. Wong, and J. H. Shapiro, Phys. Rev. Lett. **111**, 010501 (2013).
[12] Q. Zhuang and J. H. Shapiro, Phys. Rev. Lett. **128**, 010501 (2022).
[13] F. Xu, X.-M. Zhang, L. Xu, T. Jiang, M.-H. Yung, and L. Zhang, Phys. Rev. Lett. **127**, 040504 (2021).
[14] T. Gregory, P.-A. Moreau, E. Toninelli, and M. J. Padgett, Sci. Adv. **6**, eaay2652 (2020).
[15] J. Zhao, A. Lyons, A. C. Ulku, H. Defienne, D. Faccio, and E. Charbon, Opt. Express **30**, 3675 (2022).
[16] S. Barzanjeh, S. Pirandola, D. Vitali, and J. M. Fink, Sci. Adv. **6**, eabb0451 (2020).
[17] C. S. Chang, A. Vadiraj, J. Bourassa, B. Balaji, and C. Wilson, Appl. Phys. Lett. **114**, 112601 (2019).
[18] E. D. Lopaeva, I. Ruo Berchera, I. P. Degiovanni, S. Olivares, G. Brida, and M. Genovese, Phys. Rev. Lett. **110**, 153603 (2013).
[19] S. Pirandola, B. R. Bardhan, T. Gehring, C. Weedbrook, and S. Lloyd, Nat. Photonics **12**, 724 (2018).
[20] Z. Zhang, S. Mouradian, F. N. C. Wong, and J. H. Shapiro, Phys. Rev. Lett. **114**, 110506 (2015).
[21] Q. Zhuang, Z. Zhang, and J. H. Shapiro, Phys. Rev. Lett. **118**, 040801 (2017).
[22] See Supplemental Material at http://link.aps.org/supplemental/10.1103/PhysRevLett.131.033603 for experimental setup, theoretical analysis, and extra data, including Refs. [23–27].
[23] Z.-Y. J. Ou, *Multi-Photon Quantum Interference* (Springer, New York, 2007), Vol. 43.
[24] M. Lahiri, R. Lapkiewicz, G. B. Lemos, and A. Zeilinger, Phys. Rev. A **92**, 013832 (2015).
[25] B. Viswanathan, G. B. Lemos, and M. Lahiri, Opt. Express **29**, 38185 (2021).
[26] G. B. Lemos, M. Lahiri, S. Ramelow, R. Lapkiewicz, and W. N. Plick, J. Opt. Soc. Am. B **39**, 2200 (2022).
[27] Y. Ma, N. Gemmell, E. Pearce, R. Oulton, and C. Phillips, arXiv:2303.08185.
[28] X. Y. Zou, L. J. Wang, and L. Mandel, Phys. Rev. Lett. **67**, 318 (1991).
[29] G. B. Lemos, V. Borish, G. D. Cole, S. Ramelow, R. Lapkiewicz, and A. Zeilinger, Nature (London) **512**, 409 (2014).
[30] A. V. Paterova, H. Yang, Z. S. Toa, and L. A. Krivitsky, Appl. Phys. Lett. **117**, 054004 (2020).
[31] I. Kviatkovsky, H. M. Chrzanowski, E. G. Avery, H. Bartolomaeus, and S. Ramelow, Sci. Adv. **6**, eabd0264 (2020).
[32] A. V. Paterova, S. M. Maniam, H. Yang, G. Grenci, and L. A. Krivitsky, Sci. Adv. **6**, eabd0460 (2020).
[33] A. Hochrainer, M. Lahiri, M. Erhard, M. Krenn, and A. Zeilinger, Rev. Mod. Phys. **94**, 025007 (2022).
[34] A. Hochrainer, M. Lahiri, R. Lapkiewicz, G. B. Lemos, and A. Zeilinger, Optica **4**, 341 (2017).
[35] A. Zajonc, L. Wang, X. Zou, and L. Mandel, Nature (London) **353**, 507 (1991).
[36] M. O. Scully and K. Drühl, Phys. Rev. A **25**, 2208 (1982).
[37] M. O. Scully, B.-G. Englert, and H. Walther, Nature (London) **351**, 111 (1991).
[38] M. Kutas, B. Haase, J. Klier, D. Molter, and G. von Freymann, Optica **8**, 438 (2021).
[39] D. A. Kalashnikov, A. V. Paterova, S. P. Kulik, and L. A. Krivitsky, Nat. Photonics **10**, 98 (2016).
[40] A. V. Paterova and L. A. Krivitsky, Light Sci. Appl. **9**, 82 (2020).
[41] A. V. Paterova, H. Yang, C. An, D. A. Kalashnikov, and L. A. Krivitsky, Quantum Sci. Technol. **3**, 025008 (2018).
[42] A. Vanselow, P. Kaufmann, I. Zorin, B. Heise, H. M. Chrzanowski, and S. Ramelow, Optica **7**, 1729 (2020).
[43] S. Mukamel, M. Freyberger, W. Schleich, M. Bellini, A. Zavatta, G. Leuchs, C. Silberhorn, R. W. Boyd, L. L. Sánchez-Soto, A. Stefanov *et al.*, J. Phys. B **53**, 072002 (2020).

[44] M. Gilaberte Basset, A. Hochrainer, S. Töpfer, F. Riexinger, P. Bickert, J. R. León-Torres, F. Steinlechner, and M. Gräfe, Laser Photonics Rev. **15**, 2000327 (2021).
[45] S. Töpfer, M. Gilaberte Basset, J. Fuenzalida, F. Steinlechner, J. P. Torres, and M. Gräfe, Sci. Adv. **8**, eabl4301 (2022).
[46] M. Chekhova and Z. Ou, Adv. Opt. Photonics **8**, 104 (2016).
[47] T. Dresel, G. Häusler, and H. Venzke, Appl. Opt. **31**, 919 (1992).
[48] L. J. Wang, X. Y. Zou, and L. Mandel, Phys. Rev. A **44**, 4614 (1991).
[49] V. Ansari, B. Brecht, J. Gil-Lopez, J. M. Donohue, J. Řeháček, Z. c. v. Hradil, L. L. Sánchez-Soto, and C. Silberhorn, PRX Quantum **2**, 010301 (2021).
[50] A. Vallés, G. Jiménez, L. J. Salazar-Serrano, and J. P. Torres, Phys. Rev. A **97**, 023824 (2018).
[51] J. Fuenzalida, A. Hochrainer, G. B. Lemos, E. A. Ortega, R. Lapkiewicz, M. Lahiri, and A. Zeilinger, Quantum **6**, 646 (2022).
[52] M. Kumar, P. Kumar, A. Vega, M. A. Weissflog, T. Pertsch, and F. Setzpfandt, Appl. Phys. Lett. **119**, 244001 (2021).
[53] Y. Mukai, R. Okamoto, and S. Takeuchi, Opt. Express **30**, 22624 (2022).
[54] A. V. Paterova, Z. S. Toa, H. Yang, and L. A. Krivitsky, ACS Photonics **9**, 2151 (2022).
[55] R. W. Andrews, R. W. Peterson, T. P. Purdy, K. Cicak, R. W. Simmonds, C. A. Regal, and K. W. Lehnert, Nat. Phys. **10**, 321 (2014).
[56] H. Tu, K. Liao, Z. Zhang, X. Liu, S. Zheng, S. Yang, X. Zhang, H. Yan, and S. Zhu, Nat. Photonics **16**, 291 (2022).
[57] A. Rueda, W. Hease, S. Barzanjeh, and J. M. Fink, npj Quantum Inf. **5**, 108 (2019).
[58] T. Ono, G. F. Sinclair, D. Bonneau, M. G. Thompson, J. C. Matthews, and J. G. Rarity, Opt. Lett. **44**, 1277 (2019).
[59] S. Barzanjeh, S. Guha, C. Weedbrook, D. Vitali, J. H. Shapiro, and S. Pirandola, Phys. Rev. Lett. **114**, 080503 (2015).
[60] M. Wehner, M. Ulm, and M. Wegener, Opt. Lett. **22**, 1455 (1997).
[61] C. A. Pallikarakis, J. M. Huntley, and P. D. Ruiz, J. Opt. Soc. Am. A **37**, 1814 (2020).
[62] Z. Wang, B. Potsaid, L. Chen, C. Doerr, H.-C. Lee, T. Nielson, V. Jayaraman, A. E. Cable, E. Swanson, and J. G. Fujimoto, Optica **3**, 1496 (2016).
[63] A. Heuer, R. Menzel, and P. W. Milonni, Phys. Rev. A **92**, 033834 (2015).
[64] A. C. Cardoso, L. P. Berruezo, D. F. Ávila, G. B. Lemos, W. M. Pimenta, C. H. Monken, P. L. Saldanha, and S. Pádua, Phys. Rev. A **97**, 033827 (2018).